NJC

PAPER

View Article Online
View Journal | View Issue

Cite this: *New J. Chem.*, 2016, 40, 6834

A combined experimental and theoretical approach to study SmC → N_{cybC} phase transition in a four-ring bent-core liquid crystal†

Swapnil Singh,[a] Rahul Deb,[b] Nirmalangshu Chakraborty,[b] Harshita Singh,[a] Vineet Gupta,[a] Kirti Sinha,[a] Poonam Tandon,*[a] Myroslava Omelchenko,[c] Nandiraju Venkata Satyanarayana Rao[b] and Alejandro Pedro Ayala[d]

Received (in Montpellier, France) 19th March 2016,
Accepted 30th May 2016

DOI: 10.1039/c6nj00892e

www.rsc.org/njc

A newly synthesized four-ring bent-core liquid crystal (BCLC) has been studied using experimental and quantum chemical approach. Differential scanning calorimetry (DSC), polarised optical microscopy (POM), and X-ray investigations were carried out to identify the phase transitions and associated phases. DSC along with POM revealed four phase transitions *i.e.* Cr → SmX → SmC → N_{cybC} → Iso in the temperature range from 30 °C to 180 °C. The existence of smectic C like fluctuations also known as cybotactic groups in the broad temperature range of the nematic phase was confirmed by small angle X-ray diffraction. Conformational and vibrational analyses have been performed using density functional theory (DFT), to identify the most stable conformer having a bent shape. Analysis of the potential energy surface (PES) for different torsional angles revealed the most probable conformational states for the BCLC. Temperature dependent Fourier transform infrared (TD-FTIR) spectroscopy is used to study phase transitions and revealed marked changes in the spectral line shape especially the vibrations of OH, CH_2, CH_3, C═O, and HC═N groups during the SmC → N_{cybC} phase transition above ~95 °C. A good agreement between the calculated and observed infrared spectra validates the structure of this conformer that has been used for further studies.

1. Introduction

The discovery of novel mesomorphic phases in achiral bent- or banana-shaped molecules with unusual properties unknown for other materials *viz.* supramolecular chirality, biaxiality, ferroelectric, antiferroelectric and nonlinear optical properties,[1,2] orthogonal polar smectic phases, *etc.* created interest among scientists working in the area of liquid crystals (LCs) due to their promising applications such as the memory effect, the formation of stable fibres, bent-core organic semiconductors, molecular switching and strong photoluminescence.[3–6] The majority of bent- or banana-shaped compounds exhibiting so-called smectic phases[7] are realised in five- or more-aromatic-phenyl-ring systems with different linking groups in particular azo, ester and imine linkages. Very few of them exhibit rare biaxial nematic phases[8] (with arguments in favour and against their existence) and cybotactic nematic phases.[9,10] The formation of the nematic phase by these bent-core compounds is restricted by the constraints imposed by the bent-shape of the molecules, *i.e.*, steric hindrance for free rotation and core-core interactions promoting layer formation due to the segregation of extended aromatic moieties and end alkyl chains, as well as the incompatibility between the bent aromatic cores and aliphatic moieties. Hence, the design and synthesis of a bent-core (BC) compound with three[11] or four-ring[12] bent-core molecules exhibiting nematic phases with smectic-C (SmC) fluctuations (cybotactic groups) is a challenging task. The molecules of BCLCs consist of three parts, *i.e.* central bent-core units, terminal chains and linking groups. One of the important aspects is the nature and size of the substituent in the central core, which largely influences the mesophase behaviour.[13,14] The variation in the length of the alkoxy terminal chains not only affects the formation of liquid crystalline phases exhibited by the BC compounds, but also physical properties such as the dielectric anisotropy, birefringence,[15] and elastic constants.

Very few reports appeared in the literature to study the molecular structure, conformation and phase transitions in liquid crystals[16–19] using density functional theory (DFT) and

[a] *Department of Physics, University of Lucknow, Lucknow-226007, India. E-mail: poonam_tandon@yahoo.co.uk*
[b] *Chemistry Department, Assam University, Silchar-788011, Assam, India*
[c] *Department of Chemistry, Warsaw University, Al. Zwirki i Wigury 101, 02-089 Warsaw, Poland*
[d] *Departamento de Física, Universidade Federal do Ceará, C.P. 6030, 60.455-900 Fortaleza, CE, Brazil*

† Electronic supplementary information (ESI) available. See DOI: 10.1039/c6nj00892e

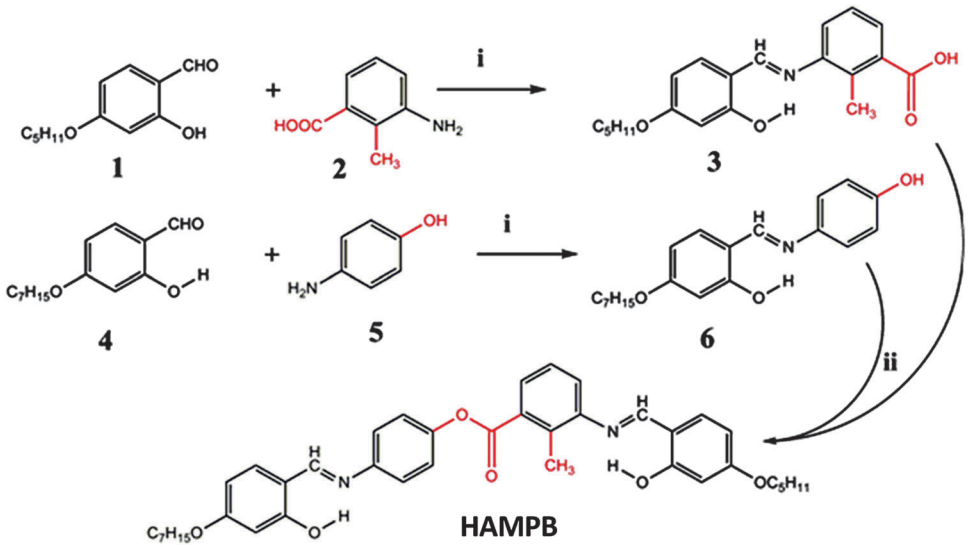

Scheme 1 *Reagents and conditions* (i) ethanol, drops of glacial acetic acid, reflux, 4 h; (ii) DCC, DMAP, DCM, 24 h.

vibrational spectroscopy. Temperature dependent Fourier transform infrared (TD-FTIR) spectroscopy is a precise and sensitive tool for monitoring the structural, rotational or conformational (torsional) changes in molecules during phase transitions.[19,20] The crystal → mesophase → isotropic transitions and *vice versa* result in the change in molecular assemblies and their conformations (that causes a change in inter/intramolecular interactions) and thereby changes in the dipole moment of the molecule. Therefore, FTIR became a sensitive detection technique for the investigation of phase transitions. The fingerprint region is very informative regarding the structural changes and provides specific information about the core (phenyl rings) and linking or functional groups (ester and Schiff base) of the molecules exhibiting liquid crystalline phases. The peak position, peak height and peak width are temperature sensitive, and therefore, very useful (especially for the liquid crystals) to investigate the dynamics of the molecule during the phase transition.

Here we report the synthesis of a newly designed four-ring BCLC system possessing an ester moiety between two phenyl rings as the central core connected through imine linkages on both sides to a phenyl ring on either side substituted with an unequal distribution of the 4-*n*-alkoxy groups (different aliphatic alkoxy end-chain lengths). Phase transition temperatures with associated enthalpies were detected by differential scanning calorimetry (DSC), and the mesophases were identified using a polarised optical microscope (POM) and confirmed by X-ray investigations. The analysis of the potential energy surface (PES) for different torsional angles revealed the most probable conformational states for the BCLC reported here, as well as provided a basic idea to understand the dynamics of the molecules during the phase transitions. Temperature dependent Fourier transform infrared spectroscopy (TD-FTIR) along with DFT is used for understanding the mechanism of phase transitions and the concomitant changes at the molecular level. TD-FTIR studies revealed prominent changes in the bands to give a sharp signature during SmC → N_{cybC} phase transition. The correlation between the infrared spectral and structural changes accompanying the phase transitions in liquid crystals at the molecular level to depict the intra- and intermolecular interactions is also presented.

2. Experimental and theoretical methodology

2.1 Synthesis

The schematic representation of the synthesis of newly designed four-ring bent-core compound [4-(*N*-4′-*n*-heptyloxysalicylidene)-aminophenyl]-[2-methyl-3-(*N*-4′-*n*-pentyloxysalicylideneamino)]-benzoate (hereafter abbreviated as HAMPB) is presented in Scheme 1. The details of the synthetic procedures of intermediate compounds **3** and **6** are presented in the ESI.† The synthesis of HAMPB is described as follows. To a solution of 2-methyl-3-*N*-(4-*n*-pentyloxysalicylideneamino)benzoic acid **3** (0.65 g, 0.002 mol) and 4-*N*-(4-*n*-heptyloxysalicylideneamino)-phenol **6** (0.68 g, 0.002 mol) in dichloromethane (DCM, 80 ml) were added dicyclohexylcarbodiimide (DCC, 0.49 g, 0.0024 mol) and 4-dimethylaminopyridine (DMAP, 20 mg).

The resulting reaction mixture was stirred at room temperature for 48 h. The urea which formed during the reaction was removed by filtration and the DCM was evaporated *in vacuo*. The solid residue of the compound was purified by column chromatography on silica gel using petroleum ether/ethyl acetate (97 : 3 v/v) as an eluent and then recrystallized from absolute ethanol and again from ethanol providing 0.58 g (yield 45%) of the target liquid crystal HAMPB as a pale-yellow solid. IR ν_{max} in cm^{-1}: 1618 ($\nu_{CH=N}$, imine); 1746 ($\nu_{C=O}$, ester), 3435 (ν_{O-H}, H-bonded); ^1H NMR ($CDCl_3$, 400 MHz): δ = 13.65 and 13.54 (s, 2H, –OH); 8.55 and 8.46 (s, 2H, –CH=N–); 8.00 (d, 1H, J = 7.2 Hz, ArH); 7.39 (t, 1H, J = 7.2 Hz, ArH); 7.37 (d, 2H, J = 8.0 Hz, ArH); 7.10–7.07 (m, 3H, ArH); 7.25 (d, 2H, J = 8.0 Hz, ArH);

6.54 (dd, 4H, J = 2.4 Hz, 7.2 Hz, ArH); 4.01 (t, 4H, J = 6.0 Hz, –O–CH_2–); 2.69 (s, 3H, Ar–CH_3); 1.82–1.78 (pen, 4H, J = 6.2 Hz, –CH_2–CH_2–); 1.46 (q, 4H, –CH_2–CH_2–); 1.34–1.24 (m, 8H, –$(CH_2)_2$–); 0.90 (t, 6H, J = 6.9 Hz, –CH_3). Elemental analysis calculated for $C_{40}H_{46}N_2O_6$: C = 73.82%; H = 7.12%; N = 4.30%. Found C = 73.71%; H = 7.01%; N = 4.21%.

2.2 Instrumentation details

The thermal behaviour of the compound was investigated by differential scanning calorimetry (DSC). Phase transition temperatures and associated enthalpies were determined using a DSC 821e (Mettler Toledo, Switzerland) operating with version 5.1 of stare software. Accurately weighted samples (2.22 mg) were encapsulated in aluminium pans having pierced lids to allow escape of volatiles. The sample was heated from 30–180 °C followed by cooling with the scanning rate of 5 °C min^{-1} employing nitrogen purging at the rate of 80 ml min^{-1}. The temperature axis and the cell constant were calibrated using indium.

The transition temperatures along with the phase identification of the sample HAMPB were determined using a polarising optical microscope (POM) (Nikon Optiphot-2-pol) attached with a hot and cold stage, HCS302, and with an STC200 temperature controller, from INSTEC Inc. USA. The small angle X-ray diffraction (SAXRD) patterns were obtained using a Bruker Nanostar system. The cybotactic groups in the nematic phase were investigated for samples aligned in a magnetic field, by X-ray diffraction. The CuKα (1.54 Å) radiation and the Goebel mirror type monochromator were used and the patterns were registered using an area detector VANTEC2000. The broad range diffraction was obtained using a Bruker GADDS system working with CuKα (1.54 Å) radiation.

Temperature dependent infrared spectra of the sample HAMPB were recorded on a Vertex 70 Fourier transform infrared spectrometer (Bruker, Ettlingen, Germany) within the 4000–400 cm^{-1} spectral region in both heating and cooling cycles. KBr pellets of solid samples were prepared from mixtures of KBr and the sample in a 200 : 1 ratio using a hydraulic press. Attenuated total reflectance and diffuse reflectance sampling techniques provided similar spectra. A liquid-nitrogen cryostat (Janis Research, Wilmington, USA) was employed to record FTIR spectra as a function of temperature.

2.3 Computational methodology

The initial geometry optimization of HAMPB was done by employing DFT calculations using GAUSSIAN 09 software[21] following the 6-31G(d) basis set and the Becke3-Lee–Yang–Parr (B3LYP) hybrid functional[22–24] that take account into electron correlations. The basis set 6-31G(d) augmented by '*d*' diffuse functions on heavy atoms was used.[25,26] The conformational analysis of the HAMPB molecule has been performed at the same level of theory. In order to find the most stable structure as well as the possible conformers, assuming ordered side chains (all *trans*) and relaxing the geometry, the one dimensional PES of torsional angles has been performed along all the dihedral angles ϕ1–ϕ14. A complete set of 276 internal coordinates were defined using Pulay's recommendations.[27,28] The molecule HAMPB belongs to the C1 point group, as it does not exhibit any unique symmetry. To compare the calculated spectrum with the observed spectrum at room temperature, they were scaled down using only one scaling factor (0.9614).[29] The vibrational assignments of the normal modes were done using potential energy distribution (PED) of each mode in terms of the internal coordinates using localized symmetry and utilizing GAR2PED[30] software. The calculated infrared spectrum was simulated by adopting a pure Lorentzian band profile (FWHM = 8 cm^{-1}). CHEMCRAFT[31] and GAUSSVIEW 5.0[32] software were used to visualize the calculated molecular vibrations and confirmations. PeakFitv4.1 software was used for the analysis of the peak position, intensity and width (FWHM) of the observed temperature-dependent FTIR spectra.

3. Results and discussion

3.1 Mesomorphic properties: molecular design, thermal analysis and phase characterization

A newly designed four-ring bent-core compound HAMPB exhibiting liquid crystalline phases was successfully synthesized and characterized. These molecules are well designed to possess two hydroxyl groups in the *ortho* position to imine linkage in both the wings, to participate in intramolecular H-bonding. The imine linkages are stabilized by H-bonding due to the presence of the *o*-hydroxyl group of the phenyl ring in both the wings. The presence of the *ortho* hydroxyl group in benzylidene moieties enhances the stability of imines through intramolecular H-bonding to overcome the hydrolytic instability of the molecules towards atmospheric hydrolysis as well as promotes extended conjugation in the core and also enhances the transverse dipole-moment. Hence the resorcylidene core is more stable towards atmospheric hydrolysis. The ester group also plays an important role and is involved in the conformational changes during the phase transition. The transition temperatures and associated enthalpies are determined from the DSC studies both in second heating and cooling cycles. The identification of mesophases was carried out using POM studies and the identified phases are confirmed by the complementary technique of X-ray diffraction studies.

The compound HAMPB exhibits three enantiotropic liquid crystalline phases in the temperature range of 30–180 °C. The phase transition temperatures, entropy and enthalpy changes were measured in both heating and cooling scans at a scan rate of 5 °C min^{-1} and are presented in Table 1. Upon heating the sample four endothermic peaks appeared (Fig. 1) that correspond to the four phase transitions Cr → SmX → SmC → N_{cybC} → Iso (confirmation of phases is described below). The large value of the enthalpy (17.3 kJ mol^{-1}) at 89.66 °C confirmed a first order transition of the sample from a crystalline phase to a liquid crystal phase. The large enthalpy and entropy values suggested order to disorder transition reflecting the changes in the packing of molecular structure. However the small values of both enthalpy and entropy associated with the three other transitions are considered to be the changes in the molecular structural arrangement of layer order and orientational order reflecting the

Table 1 Phase transition temperatures (°C) of the compounds HAMPB recorded for second heating (first row) and second cooling (second row) cycles at 5 °C min^{-1} from DSC. The enthalpies (ΔH in kJ mol^{-1}) and entropies (ΔS in J mol^{-1} K^{-1}) are presented in parentheses

Cr	SmX	SmC	N_{cybC}	I	ΔT
• 89.66 (24.1, 66.6)	• 93.98 (0.47, 1.29)	• 98.14 (0.78, 2.10)	• 171.65 (0.50, 1.12)	•	81.99
• 64.23 (17.3, 51.5)	• 77.52 (1.15, 3.27)	• 93.61 (0.51, 1.39)	• 171.87 (0.38, 0.86)	•	107.64

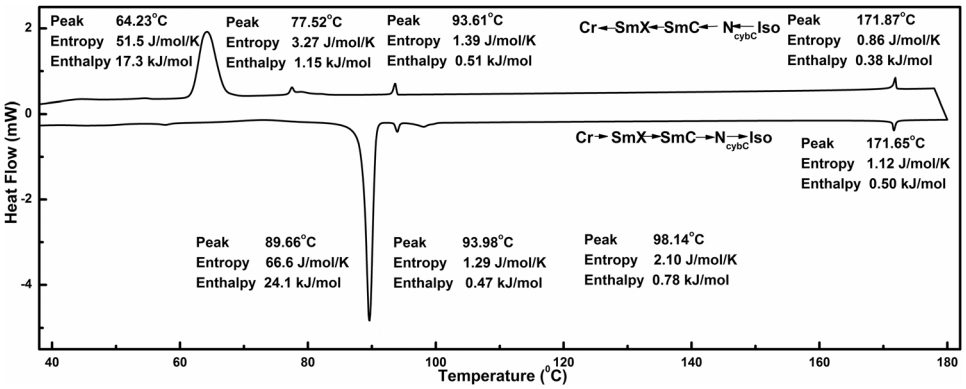

Fig. 1 DSC thermograph of the compound HAMPB for heating (downward curve) and cooling (upward curve) cycles at 5 °C min^{-1}. The enthalpies (ΔH in kJ mol^{-1}) and entropies (ΔS in J mol^{-1} K^{-1}) are also presented.

intermolecular interactions and conformational changes. In the cooling cycle also all the four exothermic peaks are observed corresponding to the transitions from Iso → N_{cybC} → SmC → SmX → Cr. Except the peak at isotropic to nematic phase transition all the three other transitions have shown supercooling by ~5 °C at N → SmC phase transition, ~16 °C at SmC → SmX phase transition and ~25 °C at SmX → Cr phase transitions. Similar changes are observed in the heating as well as cooling cycles that suggested the enantiotropic nature of the liquid crystal phase transitions. The identification of the mesophase is done by utilizing POM. These mesophases are further confirmed by the small angle X-ray technique that will be discussed in the next section.

POM studies revealed three liquid-crystalline phases (N_{cybC}, SmC and SmX) both in cooling and heating cycles between the crystalline phase and the isotropic phase. The sample sandwiched between an untreated glass plate and a coverslip, upon cooling from the isotropic phase, exhibited typical threaded (Fig. 2a) and Schlieren (Fig. 2b) textures with characteristic two brush defects (s = 1/2) and four brush defects (s = 1). The presence of a large number of s = 1/2 defects is typically exhibited by the nematic phase and is quite unique and characteristic of

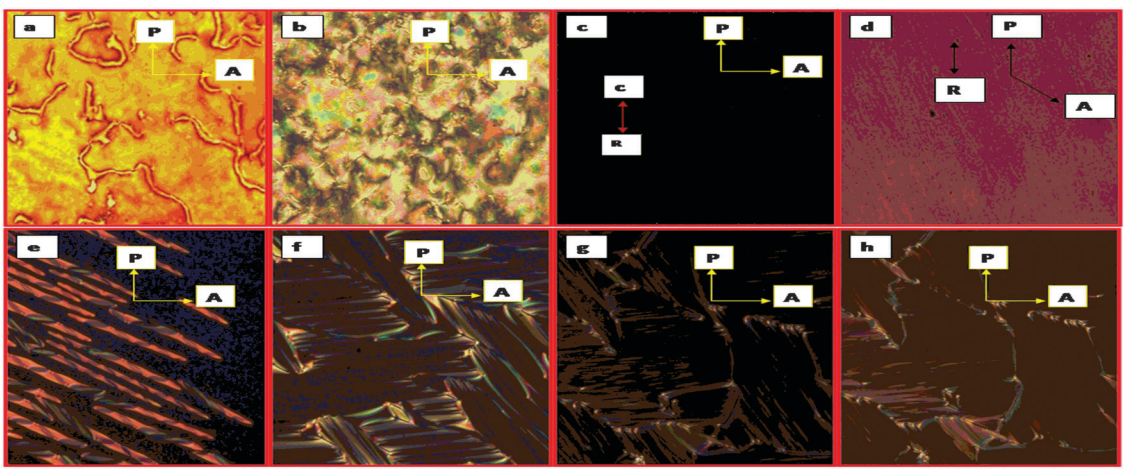

Fig. 2 POM investigations between crossed polarizers upon cooling with an untreated glass plate and a cover slip (a) Marble texture in the N_{cybC} phase at 171.5 °C. (b) Schlieren texture with growth of dark region characteristics of N_{cybC} at 164.1 °C. Optical texture in thin cells of 5 m (c and d) by PI treatment for homogeneous alignment (c) Optical texture extinction at 94 °C. (d) With the analyser rotated 45° from the optic axis direction at 94 °C. (e) Rope-like texture during transition at 93.6 °C from the nematic phase to the SmC phase. (f) SmC phase broken fan-like texture at 93.2 °C. (g) SmX phase focal conic fan texture at 77.5 °C with characteristic boundaries between two different domains of molecular alignment. (h) Upon further cooling a texture with increased birefringence at 74.9 °C.

bent-core materials exhibiting the nematic phase. However, they are rarely observed in the nematic phase exhibited by rod-like compounds as they escape into three dimensions.[33,34] Upon further cooling, they exhibit a slow transition to a homeotropic alignment of molecules initially over small areas which subsequently spread to the entire area under observation and such anchoring transition at which molecules aligned perpendicular to the surface indicating the cybotactic cluster formation is commonly observed in nematic phases exhibited by bent-core compounds.[9,10,33,34]

Upon slow cooling from the isotropic phase in thin cells of 5 μm with polyimide treated glass substrates, the sample appeared black (Fig. 2c), a defect-free planar texture, with the director (optic axis) of the nematic phase was aligned with one of the polarizer directions in POM studies, such that the high-temperature phase resembled a birefringent plate of a crystal with the optic axis in the plane of the substrate. With the variation of the sample in the azimuthal angle, the transmitted light intensity between crossed polarizers continuously increased to a maximum (Fig. 2d), when the optic axis was oriented at 45°. Characteristic flickering was observed upon tapping the sample caused by the Brownian motion of the director that is characteristic of the nematic phase with strong, long living director fluctuations. Upon further cooling a low-temperature mesophase (designated as SmC) with rope-like texture (Fig. 2e) which grows slowly to form broken focal conic fan texture with stripe patterns (Fig. 2f) appeared at 93.4 ± 0.2 °C with a transitional entropy ($\Delta S_{N_{cybC}-SmC}/R = 0.16$). The small transitional entropies at both the transitions (N_{cybC} → SmC and SmC → SmX) and the two-phase coexistence of ~0.1 °C at these transitions observed in POM investigations can be attributed to weakly first-order phase transitions. Upon further cooling the broken fan-like texture transformed to larger domains with boundaries (Fig. 2g). Within each of these domains, birefringence increased upon further cooling (Fig. 2h). The phase exhibited clear dark and bright domains. The brightness of the domains interchanges when one of the polarizers is uncrossed in the opposite direction, indicating the birefringent nature of this phase. The nematic phase in these unsymmetrical achiral bent-core compounds resembled the nematic cybotactic phase.[9,10,33,34]

The sample was further studied by small and wide angle X-ray diffraction. In the nematic phase the X-ray signal, related to the molecular length, is significantly broader than in the smectic or crystal phase (that appeared below the nematic phase) that is the signature of the short range positional order of molecules in this phase (Fig. 3a and b). The sample aligned by the magnetic field in the nematic phase showed azimuthal splitting of the low angle signal as shown in Fig. 3b. The corresponding X-ray intensity profile in a nematic phase at 100 °C was aligned by the magnetic field showing the azimuthal splitting of the signals in the low angle region as depicted in Fig. 3c, related to the molecular length that is characteristic of the local SmC type order, Fig. 3b. The schematic description of the aligned molecules with their long axes along the magnetic field is shown in Fig. 3d while the local layer normal is tilted from the magnetic field and such smectic fluctuations are called 'cybotactic groups'.[34] The X-ray experiment confirmed that the transition at around ~93 °C is related to the developing lamellar structures. The X-ray diffraction signal in the wide angle region confirmed that the nematic and smectic phases had a liquid-like in-plane order, as the signal corresponding to 4.5 Å (the transverse distance between molecules) remains diffused. Hence, the X-ray investigations complimented the POM studies to confirm LC phases as the cybotactic nematic (N_{cybC}) and SmC phases. Even though the SmC → SmX phase transition was detected by DSC, the same could not be detected by X-ray studies due to the fast recrystallization of the sample (~77 °C). The observed POM texture in the thin film (~74 °C) is a super-cooled phase texture of the SmC phase.

3.2 Density functional theory: molecular geometry optimization and conformational analysis

The combined temperature dependent FTIR spectroscopy and DFT calculations have been used for the investigation of hydrogen bonding as well as the dynamics of the molecules during the phase transitions. The vibrational assignments are made for the correct peak identification of the observed IR spectra, on the basis of the calculated potential energy distribution, the peak intensity value and the presence/absence of peaks in molecules having similar groups.

DFT calculations of HAMPB were performed to obtain the optimized molecular structure. In order to find the most stable conformer the conformational analysis has been performed by employing the DFT/B3LYP/6-31G(d) level of theory followed by initial geometry optimization and shown in Fig. 4. The one-dimensional potential energy surface scan (PES) of the torsional angles, relaxing the geometry on the energy minimised conformation, has been performed along all the dihedral angles ϕ1–ϕ14 (as labelled in Fig. 4), assuming ordered side chains (all *trans*), and the PES as a function of dihedral angle is presented in Fig. 5. Total 45 conformers were obtained and out of them, 28 conformers are the same in energy and having a similar structure. Now remaining 18 (Fig. S1, ESI†) conformers are under investigation and on account of their energy, the lowest energy (−2112.84681 Hartree) conformer is named conformer I, the second lowest is named conformer II and so on (Fig. 6). Conformer I is the most stable conformer and exhibits a banana shape that validates our conformational analysis (Fig. S2, ESI†). Upon analyzing all the 18 conformers, it is found that conformers I to VIII have a relatively low energy ranging from 0.00 to 0.88 kcal mol^{-1} while conformers IX–XVII have a much higher relative energy and cannot exist even in the isotropic phase.

Thus, further computations are done for conformer I. The geometrical parameters such as the bond length, the bond angle and the dihedral angle of the conformers I have been tabulated and presented in Table S1 (ESI†). In this conformer, the H atom of the hydroxyl group (H55 and H2) participates in the strong intramolecular hydrogen bonding O–H···N with the N atom of Schiff base (N56 and N1) that results in a planar six-membered ring. The hydroxyl group (OH) and Schiff base (HC═N) are substituted on the phenyl rings R1 and R4 while the methyl group (CH_3) is attached to ring R3 (can be seen clearly from Fig. S2, ESI†). All the four rigid phenyl rings are non-planar in conformer I, the torsion angles between the

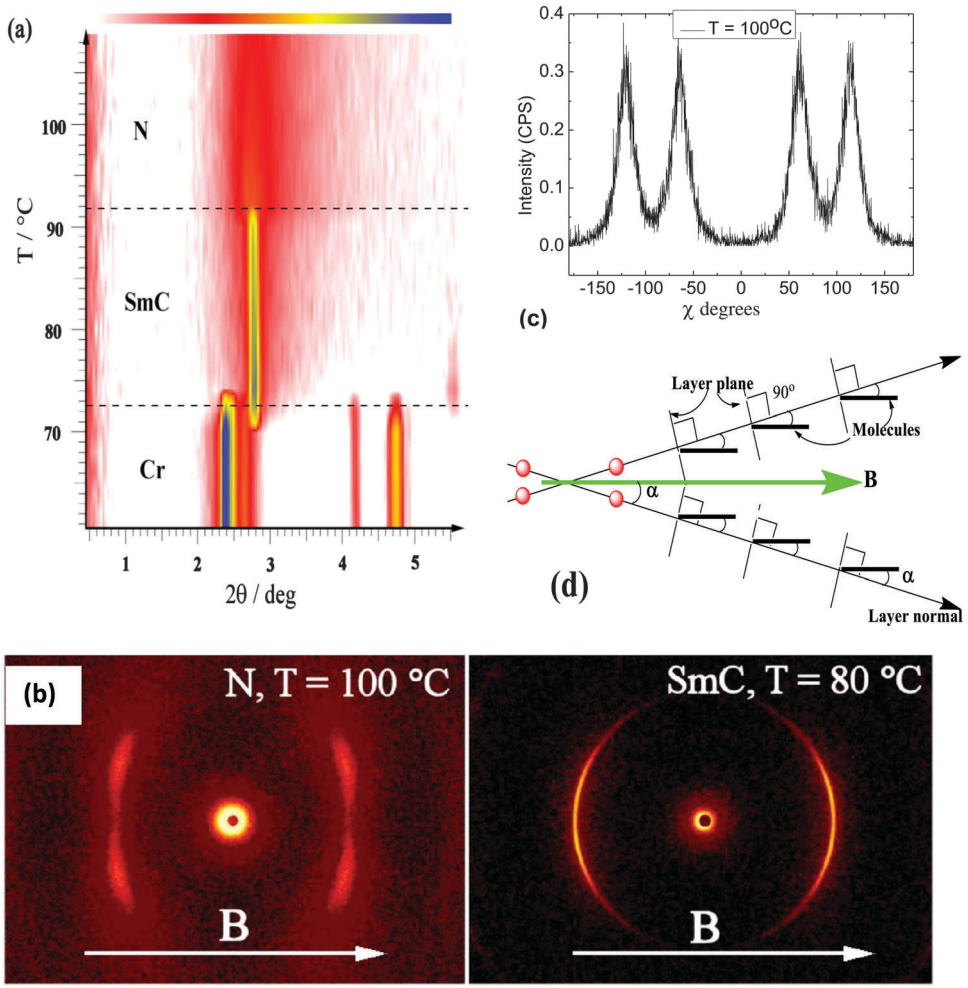

Fig. 3 (a) Temperature dependence of the signal position on 2q *vs.* temperature, obtained by small-angle X-ray diffraction, upon slow cooling the sample in cybotactic nematic, SmC and crystal phases, and (b) the 2D X-ray pattern obtained for the sample aligned by the magnetic field in nematic and smectic phases (the arrow indicates the direction of the field). (c) Corresponding X-ray intensity profile in the nematic phase at 100 °C aligned by the magnetic field showing the azimuthal splitting of the signals in the low angle region. (d) Schematic picture showing the geometry of layers, molecules and X-ray signals in the nematic phase. Note that the recrystallization of the sample (74 °C) did not allow the observation of SmC → SmX phase transition detected by DSC.

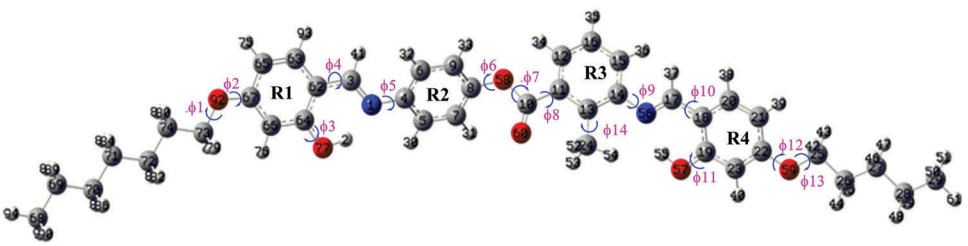

Fig. 4 Initial optimized structure.

R1 and R2, R2 and R3 and R3 and R4 are ~31°, 40° and 39°, respectively and a π-electron conjugated system can be inferred. The carbon atoms of the alkoxy chains are nearly in the same plane, which is almost coplanar with the neighbouring phenyl rings (R1 and R4). The molecular length and the bent angle of conformer I are measured to be ~3.48 nm and ~134°, respectively, using GAUSSVIEW 5.0 software. Our calculated results are in good agreement with the reported structural studies of the BCLC.[35,36]

3.3 Spectroscopic investigation

3.3.1 Vibrational assignments. In the present work the phase transitions in the HAMPB were monitored by temperature dependent infrared spectroscopy. However, it is important

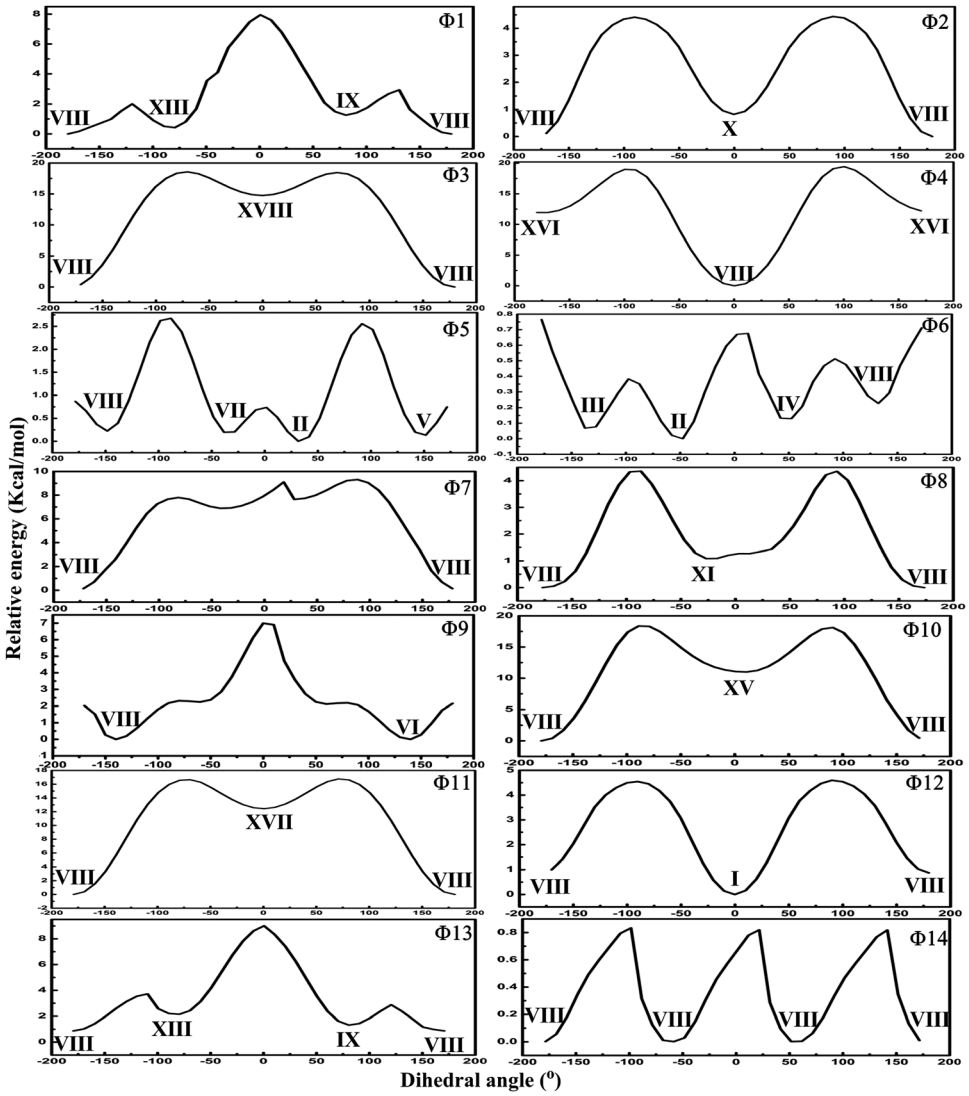

Fig. 5 The potential energy graph plotted between the relative energy (kcal mol^{-1}) and the dihedral angle (degree) presenting the possible conformers I–XVIII.

to know the precise assignment of modes before using them as marker bands. Vibrational assignments are also very useful for understanding the mechanism of transition, as they provide information about the functional groups that are affected during the transition, as associated modes will show changes upon heating and cooling.

The optimized structure of most stable conformer I is used for the calculation of vibrational spectra of the HAMPB. A comparison of the calculated and experimental room temperature infrared spectra (Fig. 7) shows a good agreement that validates the structural model used (conformer I) for calculations. All observed peaks are accurately assigned to specific vibrational modes on the basis of potential energy distribution (PED), utilizing previous reports of the vibrational mode assignments for substituted phenyl rings and alkyl chains in similar molecules[16–18] (Table S2, ESI†). The value of the correlation coefficient (R^2 = 0.99761) and the graph between the observed and calculated wavenumbers show a good agreement between them (illustrated in Fig. S3, ESI†).

It is observed that the overlapping of several CH_2 bands resulted in the broadening of the peaks in the higher region. Hence, in this region, the accurate assignment (2700–3200 cm^{-1}) is a challenging job. Therefore, the spectroscopic analysis of these stretching bands for liquid crystalline systems has not been done in many cases. The lucid signatures of the crystal modification are observed in this region.[37] There are four distinct peaks of methyl and methylene asymmetric and symmetric stretching. The higher frequency region, 2800–3500 cm^{-1}, reveals the presence of CH_3/CH_2 stretching vibrational modes along with ring CH and OH stretching modes. The CH_3 asymmetric stretching (hereafter abbreviated as r^-) and symmetric stretching (hereafter abbreviated as r^+) modes were assigned to the shoulder peaks at 2951 and 2870 cm^{-1}, respectively. The CH_2 asymmetric stretching (hereafter abbreviated as d^-) and symmetric stretching (hereafter abbreviated as d^+) modes were observed as intense peaks at 2930 and 2857 cm^{-1}, respectively. It is well known that d^+ and d^- are strong indicators of the chain conformation. The *ortho*-substituted hydroxyl group stretching vibrations showed

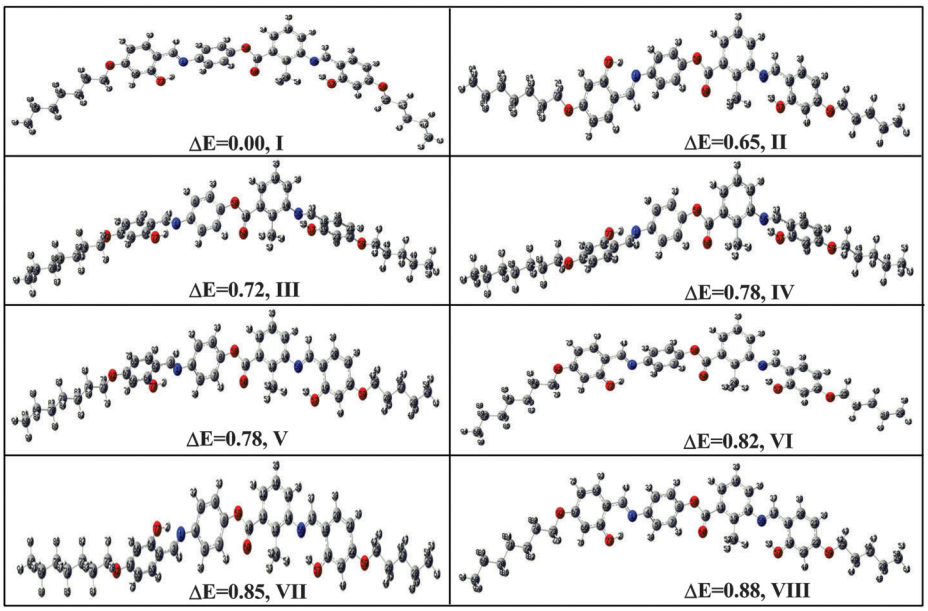

Fig. 6 The first 8 conformers with their relative energy (kcal mol^{-1}).

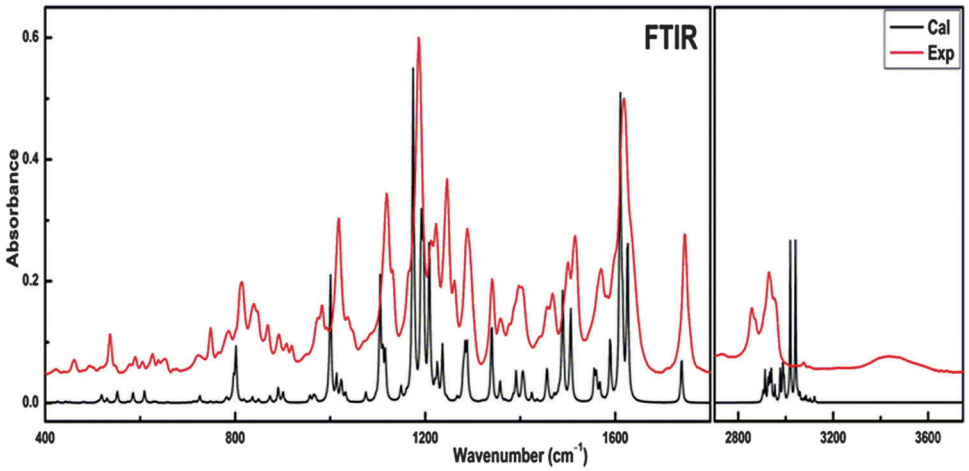

Fig. 7 Observed and calculated (scaled) infrared spectrum of HAMPB, at room temperature in the higher region (3700–2800 cm^{-1}) and the lower region (1800–400 cm^{-1}).

the involvement in intramolecular hydrogen bonding with imine linkage that lies in the region 3400–3450 cm^{-1}.[35,38] A broad peak at 3435 cm^{-1} was assigned to the OH stretching. Three small peaks at 3098, 3074 and 3042 cm^{-1} correspond to the ring CH stretching vibrations.

The lower region shown in Fig. 7 revealed rich spectral signatures composed of a large number of well-defined vibrational mode absorptions. The carbonyl stretching vibrations in saturated esters are expected in the region 1750–1735 cm^{-1}. A distinct sharp intense C═O stretching peak observed at 1746 cm^{-1} suggests the nonparticipation of the C═O moiety in hydrogen bonding. Free C═N stretching vibrations lie within the range 1690–1640 cm^{-1}. However, the C═N stretching mode observed as an intense peak at 1618 cm^{-1} clearly confirmed the participation of the N atom of the imine group in intramolecular hydrogen bonding (Fig. S2, ESI†). Peaks at 1570 and 1516 cm^{-1} are associated with ring CC stretching. Peaks at 1456 and 1377 cm^{-1} are assigned to the CH_2 scissoring and CH_3 bending or umbrella mode, respectively. CH rocking and CH out-of-plane bending of Schiff base are observed at 1358 and 984 cm^{-1}, respectively. Generally the CH_2 wagging mode is observed in the region 1150–1400 cm^{-1} which corresponds to the all-*trans* structure of the alkyl chain.[39–42] Hence, the observed CH_2 wagging mode at 1396 cm^{-1} supported the all *trans* conformation of hydrocarbon chains in HAMPB. The strongest peak in this region at 1186 cm^{-1} reflects the coupled mode of ring C4–N1 stretching with ring C8–O58 stretching and trigonal deformation of the ring. The ring CH in-plane bending modes are observed at 1223, 1165, 1132, 1130 and 1119 cm^{-1} in the region 1230–1100 cm^{-1}. The CH in-plane-bending is known to

be a sensitive indicator of the phase transition[16–18] in liquid crystals. The exact shape of this band including the peak position, width, and the number of components reflects the packing arrangement of the alkyl chain assemblies. The peak at 1047 cm^{-1} corresponds to the skeletal mode of the hydrocarbon chains or C–C–C backbone stretching mode. The band at 982 cm^{-1} is assigned to the methylene CH_2 twisting mode. The band at 764 and 723 cm^{-1} corresponds to the CH_2 rocking mode. The CH out-of-plane bending modes that are observed in the region 940–780 cm^{-1} appeared at 918, 908, 868, 846, 839, 814 and 787 cm^{-1} in the observed FTIR spectrum. The difference between the calculated and observed results is due to the fact that calculations have been done on single molecule neglecting intermolecular interactions.

3.3.2 Dynamics of molecules and hydrogen bonding at phase transitions. Temperature dependent FTIR spectra have been recorded when heating the sample over the temperature range of 25–185 °C followed by cooling up to 30 °C. Changes in the spectra are observed in both heating and cooling cycles that support DSC and POM results. However, the phase transition analysis has been performed only during the heating cycle. The phase transitions Cr → SmX → SmC → N_{cybC} → Iso occurred at ~89.66 °C, 93.98 °C, 98.14 °C and 171.65 °C (from DSC) and the associated thermal activation energies are ~0.721, ~0.729, ~0.737 and ~0.884 kcal mol^{-1}, respectively. The FTIR spectra are recorded just before and after the transition temperature to identify the clear signatures of the phase transition in the spectral peaks. The phase transitions result in the change in the peak position, relative intensity and peak width (FWHM). To obtain the precise position, width and intensity of peaks, peak fitting was done using the Voigt (Lorentz + Gauss) profile. The observed peaks from the FTIR spectrum (~25 °C) are critically examined and assigned to best fit with the calculated spectrum. Upon heating the sample, distinct changes have been observed in the spectra mainly during SmC → N_{cybC} phase transition above ~95 °C as shown in Fig. 8. Further FTIR bands associated with the core showed prominent changes in spectral features (in particular line width) during the other three phase transitions (Cr → SmX, SmX → SmC and N_{cybC} → Iso) indicating that the core no longer remains rigid during these transitions. The interlinked groups and soft alkoxy chains provide flexibility to the molecule and are responsible for the rotation of the molecule that results in the conformational changes during the SmC → N_{cybC} phase transition which are clearly reflected in the spectral features. As it is evident from the structure, the title molecule may be considered to consist of two distinct parts: (a) the "core" region comprised of four phenyl rings connected by ester-imine linkages (imine-ester-imine) and (b) "aliphatic" region comprised of the terminal alkoxy chains (OC_7H_{15} and OC_5H_{11}) attached at both ends of the core. To understand the dynamics of the molecule during phase transition, especially during SmC → N_{cybC} (skewed cybotactic clusters with the fragmented SmC phase), the crystalline phase is assumed as a closely packed structure while SmX and SmC phases have pseudo-layer ordering and layered structure, respectively.

The analysis of the TD-FTIR spectra reveals that some specific modes (marker bands) respond strongly and undergo pronounced spectral changes during the phase transitions. However, the entire spectral region showed slight variation. Among them, C═O stretching showed maximum variation in the peak position (~8 cm^{-1}) during the SmC → N_{cybC} phase transition (Fig. 8). Similarly the C═N stretching mode also showed abrupt spectral changes during phase transition. The CH_2 scissoring mode at 1501 cm^{-1} is transformed into a shoulder peak upon heating. The CH_2 wagging mode at 1396 cm^{-1} changes upon heating that resulted in the weakening and broadening of the peak. The peaks at 1261, 1246, 1223 and 1213 cm^{-1} correspond to CH_2 wagging, CH_2 twisting, ring CH in-plane bending and C17C stretching, respectively and disappeared after the onset of the nematic phase with the appearance of two broad peaks at 1242 and 1225 cm^{-1}. The CH_2 twisting mode is observed at 982 cm^{-1} and diminished after heating. Peaks at 918, 908, 891,

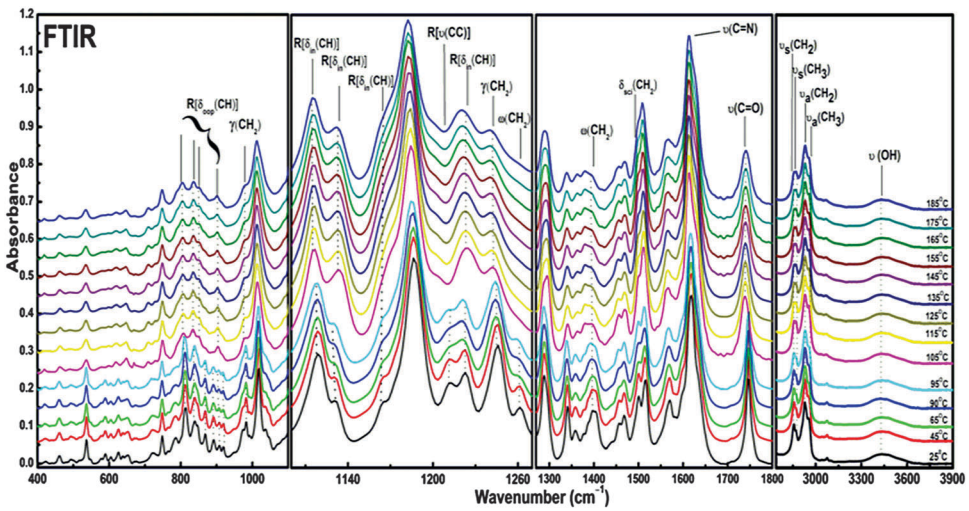

Fig. 8 Temperature dependent FTIR spectra of HAMPB recorded upon heating from the room temperature crystal phase (25 °C) to the isotropic phase (185 °C) in the region 4000–400 cm^{-1}.

868, 847, 839, 814 and 787 cm^{-1} correspond to the ring CH out-of-plane bending, start diminishing in the nematic phase and remain with only four peaks of low intensity as marked in Fig. 8. Although most of the observed peaks showed variation with the temperature, we confined our discussion to the hydroxyl group, the soft alkoxy chain and polar promesogenic linking units (C═O and C═N).

3.3.2.1 OH vibrational mode. The hydroxyl group stretching mode when involved in inter- or intramolecular hydrogen bonding appeared in the lower wave number region (3550–3200 cm^{-1}), while the free hydroxyl group peak appeared in the region 3600–3550 cm^{-1}. The observed peak position of the OH stretching mode at 3435 cm^{-1} is in good agreement with the reported results on bent-core molecules.[35,38] Further DFT optimised structures also supported a strong intramolecular hydrogen bonding between the hydroxyl groups and nitrogen of the imine moiety. Upon heating to the nematic phase, the peak is clearly visible and becomes broader (Fig. 8) without any shift in the peak position up to the isotropic phase reflecting insufficient thermal activation energy to break these hydrogen bonds. The analysis of the one-dimensional PES around $\phi 3$ and $\phi 11$ (Fig. 5) which involve the rotation of hydroxyl groups (Fig. 4) revealed that the energy barrier in both the cases is much larger and hence justified the experimental results since higher energy is required to break these strong intramolecular hydrogen bonds (see the conformers XVII and XVIII in the ESI,† Fig. S1). Hence, it can be inferred that crystal modification or conformational changes during phase transitions do not affect the environment of the hydroxyl group up to an isotropic phase.

3.3.2.2 CH_2 and CH_3 vibrational modes. The CH_2 vibrational mode and the terminal CH_3 vibrational mode of soft alkoxy chains are highly sensitive towards the phase transition due to the conformational change as well as reorganisation of end alkyl chain assemblies in the molecule. The structural disordering also results in the *trans* and *gauche* rotational isomers. The changes in the peak position of methylene and terminal methyl moieties as a function of temperature are shown in Fig. 9. Four distinct peaks are observed for methyl and methylene asymmetric and symmetric stretching modes. The shoulder peaks at 2957 and 2863 cm^{-1} correspond to the asymmetric (r^-) and symmetric (r^+) stretching of the terminal methyl moiety, respectively. Two sharp peaks at 2930 and 2855 cm^{-1} correspond to the asymmetric (d^-) and symmetric (d^+) stretching of methylene moieties, respectively. Hence, these CH_2 and the terminal CH_3 vibrational modes indicated an all-*trans* conformation of alkoxy chains with small or no significant *gauche* population.[43] Initially upon heating (25–95 °C), these modes did not exhibit any marked changes (suggesting a higher structural order that offered strong packing and intact intermolecular interactions in Cr and SmX phases) but a steady and slight change is observed in spectra at ~95 °C (SmC phase) that reflects the onset of disordering in methylene chains. All the four peaks undergo sudden changes typically at SmC → N_{cybC} phase transition to indicate changes in intermolecular interactions and relaxation in molecular packing. Small changes in methylene stretching may also be attributed either to the change in the co-planarity of the alkoxy chain and the phenyl ring and hence contribute to changes in intermolecular interaction or due to the stacking effect. As illustrated in Fig. 9 the marked changes in the peak position at above ~95 °C confirmed the SmC → N_{cybC} phase transition. As the wavenumbers of these bands are 'conformation-sensitive' and respond to changes in the *trans*/*gauche* ratio in the alkyl chains[44] the marked changes can be attributed to *trans*/*gauche* isomerism of the long alkoxy chains.

The ratio of normalized integrated intensities of d^- and d^+ is also a sensitive indicator of the structural changes during the phase transition.[44] The variation of the ratio of normalized integrated intensities of asymmetric and symmetric CH_2 stretching (I_d^-/I_d^+) as a function of temperature shown in Fig. 10 also confirmed the SmC → N_{cybC} phase transition. Initially, with an increase in temperature, this ratio constantly increases up to ~95 °C that corresponds the slight structural disordering and above this temperature, it suddenly decreases, reflecting major structural/conformational changes during the SmC → N_{cybC}

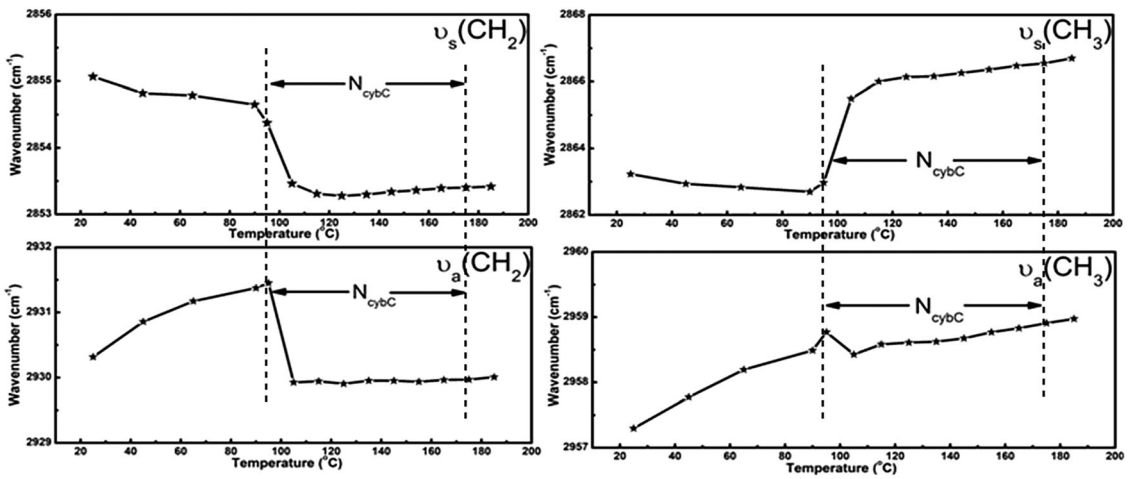

Fig. 9 Temperature dependence of the peak positions (cm^{-1}) due to asymmetric and symmetric CH_3/CH_2 stretching vibrations (3000–2800 cm^{-1}).

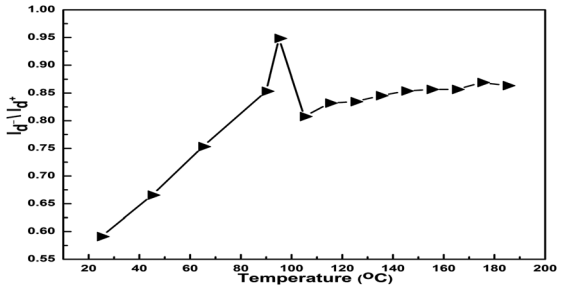

Fig. 10 Temperature dependence of the normalized integrated intensities of asymmetric and symmetric methylene (CH_2) vibrations (3000–2800 cm^{-1}).

phase transition. Upon further heating in the nematic phase the ratio is almost constant.

3.3.2.3 C═O vibrational mode. The distinct stretching mode of the carbonyl group (C═O) at ~1746 cm^{-1} (Fig. 11) undergoes a subtle change with the increasing temperature in SmX and SmC phases, in all the three parameters like the peak position, the peak width and the peak intensity and is illustrated in Fig. 12. The marked changes in peak intensity as well as ~8 cm^{-1} red shift in the peak position (~1739 cm^{-1}), which could be clearly seen from the fitted spectra (Fig. 11), clearly reflect the phase transition from the SmC → N_{cybC} phase. This red shift and broadening can be attributed to the conformational (E/Z rotational isomerism) changes due to the relative motion of the phenyl rings (R2 and R3) that further facilitates charge conjugation between the rings and carbonyl group.

Upon further heating very small but noticeable changes (Fig. 12) in the peak position (upward shift), peak intensity (downward shift in FWHM ~2 cm^{-1}) and downward trend in peak width are observed at N_{cybC} to isotropic phase transition. These upward/downward shifts are associated with the charge conjugation, conformational changes, structural changes or other inter/intramolecular interactions, *etc.*[16–18] These changes recorded in FTIR spectra can also be explained from the analysis of the PES scan of $\phi 6$ (Fig. 5). The conformers obtained along this scan (conformers II, III, IV and VIII) possess relatively low energies and exhibit smaller barrier height (Fig. 6), such that it would be possible to cross these barriers which resulted in a distinct peak shift in the C═O stretching band (~8 cm^{-1}) attributed to the molecular conformational changes around the C8–O58 bond.

3.3.2.4 C═N vibrational mode. The C═N stretching mode plays an important role in the investigation of the phase transitions as it undergoes a marked shift with the variation in temperature due to the changes in molecular dipole moment. The intensity of a peak in the infrared spectra mainly depends upon the number of components that take part in the related mode. It can be seen from Fig. 11 that only a slight variation is observed in the peak position and intensity in the low-temperature

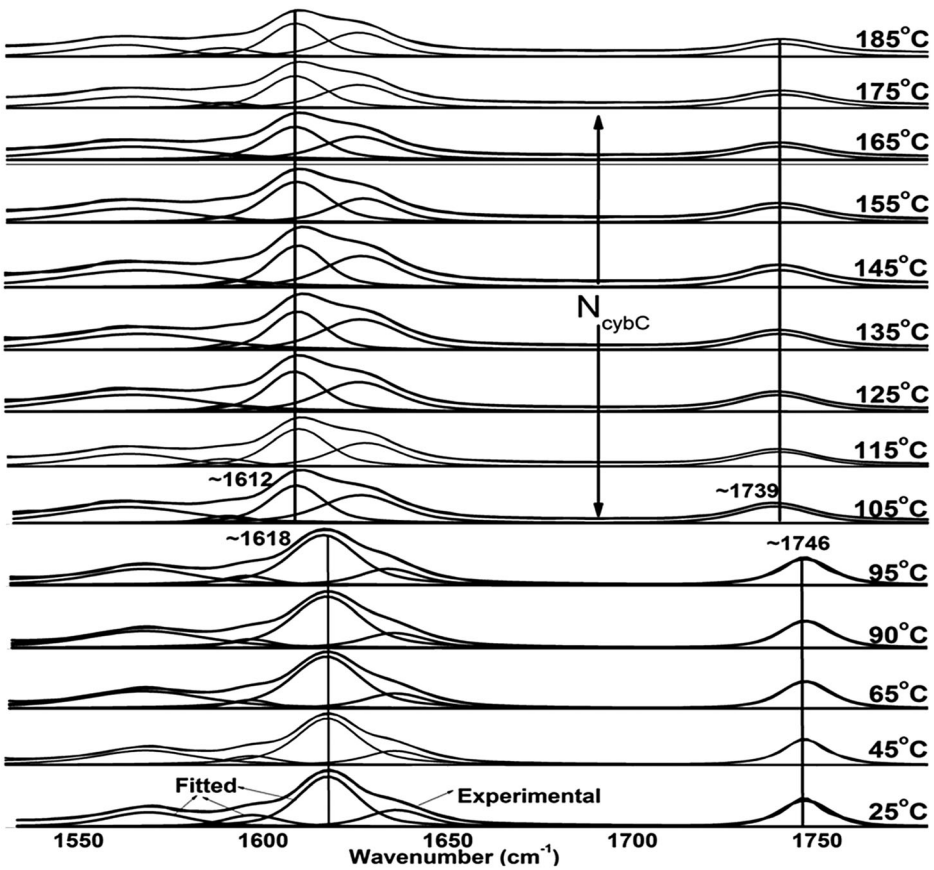

Fig. 11 Fitted infrared spectra of HAMPB, over the temperature range of 25–185 °C, for the lower region (1800–1500 cm^{-1}).

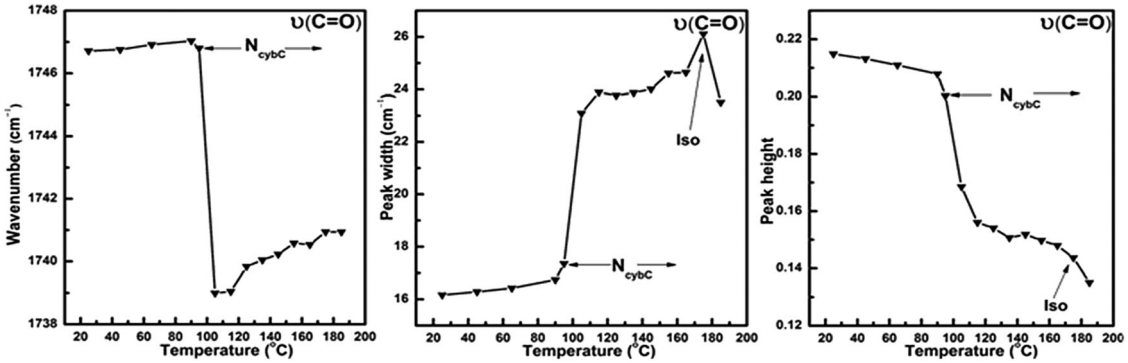

Fig. 12 Temperature dependence of carbonyl group (C═O) stretching vibration over the temperature range of 25–185 °C.

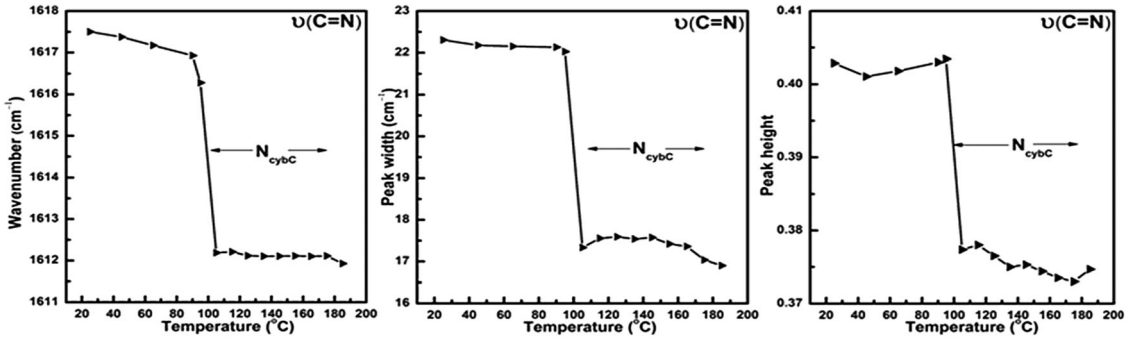

Fig. 13 Temperature dependence of C═N stretching vibration, over a temperature range of 25–185 °C.

region (25–95 °C). However, above ~95 °C, there is a red shift (~4 cm^{-1}) in wavenumber (Fig. 13) and a decrease in intensity (Fig. 13) with a decrease in FWHM (~5 cm^{-1}). Such noticeable variations suggest that the structural transformation or *E*/*Z* isomerism might be possible around the bond N–C during the phase transition.[45] Upon further heating, the peak position, as well as intensity, showed slight variations.

3.4 Reversible nature of the LC phases exhibited by the bent-core liquid crystal

The thermal reversibility of the sample was confirmed by comparing the FTIR absorptions of the title molecule at room temperature after repeated heating/cooling cycles. Comparison of the recorded spectra (Fig. 14) at ~25 °C (room temperature), ~185 °C (isotropic phase) and ~30 °C (after annealing) revealed the thermal reversibility of the sample, and prominently reflected in sensitive spectral peaks, *i.e.*, conformationally sensitive CH stretching peaks of d^+, d^-, r^+ and r^- that appeared to be distinct and intense and the C═O stretching peak with high intensity, and the reappearance of the CH out-of-plane bending mode of progression series (wagging and twisting modes). The integrated intensities are conserved in both the regions, at $(I_{30}/I_{25})_{400-1800cm^{-1}} \sim 1.01$ in the lower region as well as at $(I_{30}/I_{25})_{2600-3700cm^{-1}} \sim 0.92$ in the higher region.

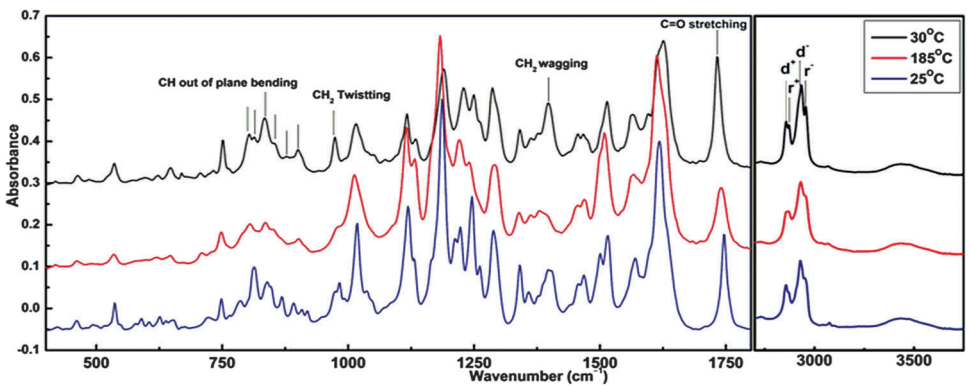

Fig. 14 Infrared spectra of HAMPB recorded at room temperature, at 25 °C (navy blue color), after annealing the sample at 185 °C (red color) and after cooling the sample at 30 °C (black color).

Temperature-induced minor but non-vanishing changes are still present in the sample that results in some shifting and broadening in the FTIR peaks due to the minor changes in the molecular conformations after annealing the sample. However, most of the FTIR peaks, POM as well as DSC data support the reversibility of the LC phases. Thus, it can be concluded that the title molecule exhibited reversible characteristics with good thermal stability.

4. Conclusion

A four-ring bent-core compound [4-(*N*-4′-*n*-heptyloxysalicylidene)-aminophenyl]-[2-methyl-3-(*N*-4′-*n*-pentyloxysalicylidene-amino)]-benzoate (HAMPB) was successfully designed, synthesized and characterized. The four-ring bent-core liquid crystal HAMPB exhibits the cybotactic nematic phase (N_{cybC}) with strong SmC like fluctuations in the wide temperature range. The long alkoxy chains are mainly responsible for these cybotactic clusters with a fragmented SmC phase structure in the nematic phase. Small angle X-ray investigations of the aligned sample in the magnetic field complemented the polarised optical microscopy and differential scanning calorimetry studies to confirm the nematic phase with SmC type fluctuations as N_{cybC} and the phase variant as SmX → SmC → N_{cybC}. A detailed conformational analysis has been carried out to find the most stable conformer followed by vibrational assignment to make correct peak identification. The calculated potential energy scan predicted 18 conformers along with the most stable conformer (conformer I) that might be expected to be closer to the real system as the molecular length and the bent angle of this conformer are nearer to the values observed in other similar systems. The theoretically calculated spectrum of conformer I showed a good agreement with experimental Fourier transform infrared spectra that validates the structure of conformer I. In addition, an accurate assignment of the peaks of the infrared spectrum (recorded at room temperature) was done to understand the changes in spectral features during the phase transitions. Differential scanning calorimetry along with polarised optical microscopy studies revealed four phase transitions *i.e.* Cr → SmX → SmC → N_{cybC} → Iso in the temperature range from 30 °C to 180 °C. During the first two transitions, temperature dependent infrared spectra show only slight changes, which indicate that slight conformational changes (due to the bulkiness of the molecule) occurred in the molecules and the entire thermal activation energy is utilized in the crystal modification or disordering in the system. However, spectral peaks show remarkable changes during the SmC → N_{cybC} transition due to the loss of the structural order, thereby resulting in conformational changes in the molecule. The convincing signatures are observed in the vibrational modes of CH_2/CH_3 stretching vibrations, C═O and C═N that strongly support conformational changes driven by the rotation of the linking groups (relative motion of phenyl rings) facilitating the charge conjugation and responsible for the changes in the infrared spectra during SmC → N_{cybC} phase transition. One of the salient features noticed is the non-involvement of the C═O moiety in inter/intramolecular hydrogen bonding. However the N atom of Schiff base (–HC═N–) as well as the hydroxyl group (–OH) is involved in hydrogen bonding up to the isotropic phase as the large shift is not observed in both the peaks. The present study demonstrated the importance of combined techniques of FTIR and DFT along with the standard techniques to identify the most stable conformer as well as conformational changes during the phase transitions. Furthermore, these experimental techniques complemented by the theoretical results are useful to understand the dynamics of the large molecules during the phase transitions.

Acknowledgements

S. S. is thankful for the support from the UGC under the BSR meritorious fellowship scheme. V. G. is thankful to the UGC under the Dr D. S. Kothari scheme. We acknowledge Prof. Ewa Gorecka for helpful discussions and providing the X-ray experimental facility.

References

1 *Liquid Crystals Beyond Displays: Chemistry, Physics, and Applications*, ed. Q. Li, John Wiley & Sons, Hoboken, NJ, 2012.
2 *Nanoscience with Liquid Crystals: From Self-organized 45 Nanostructures to Applications*, ed. Q. Li, Springer, Heidelberg, 2014.
3 Z. Hong, Y. Jin, J. H. Lee, T. H. Yoon, E. J. Choi and E. W. Lee, *J. Phys. D: Appl. Phys.*, 2011, **44**, 415304.
4 A. Jákli, D. Krüerke and G. G. Nair, *Phys. Rev. E*, 2003, **67**, 051702.
5 H. Aboubakr, M. G. Tamba, A. K. Diallo, C. V. Ackermann, L. Belec, O. Siri, J. M. Raimundo, G. H. Mehl and H. Brisset, *J. Mater. Chem.*, 2012, **22**, 23159–23168.
6 S. Balamurugan, P. Kannan, M. T. Chuang and S. L. Wu, *Ind. Eng. Chem. Res.*, 2010, **49**(16), 7121–7128.
7 P. DeGennes and J. Prost, *The Physics of Liquid Crystals*, Oxford University Press, Oxford, 2nd edn, 1993.
8 L. A. Madsen, T. J. Dingemans, M. Nakata and E. T. Samulski, *Phys. Rev. Lett.*, 2004, **92**(14), 145505.
9 L. Chakraborty, N. Chakraborty, D. D. Sarkar, N. V. S. Rao, S. Aya, K. V. Le, F. Araoka, K. Ishikawa, D. Pociecha, E. Gorecka and H. Takezoe, *J. Mater. Chem. C*, 2013, **1**, 1562–1566.
10 G. Shanker, M. Nagaraj, A. Kocot, J. K. Vij, M. Prehm and C. Tschierske, *Adv. Funct. Mater.*, 2012, **22**, 1671–1683.
11 W. Weissflog, U. Dunemann, S. F. Tandel, M. G. Tamba, H. Kresse, G. Pelzl, S. Diele, U. Baumeister, A. Eremin, S. Stern and R. Stannarius, *Soft Matter*, 2009, **5**, 1840–1847.
12 R. Deb, R. K. Nath, M. K. Paul, N. V. S. Rao, F. Tuluri, Y. Shen, R. Shao, D. Chen, C. Zhu, I. I. Smalyukh and N. A. Clark, *J. Mater. Chem.*, 2010, **20**, 7332–7336.
13 U. Dunemann, M. W. Schroder, R. A. Reddy, S. Diele, G. Pelzl and W. Weissflog, *J. Mater. Chem.*, 2005, **15**, 4051–4061.
14 G. Dantlgraber, D. Shen, S. Diele and C. Tschierske, *Chem. Mater.*, 2002, **14**, 1149–1158.

15 Y. Arakawa, S. Nakajima, S. Kang, M. Shigeta, G. Konishia and J. Watanabe, *Liq. Cryst.*, 2012, **39**, 1063–1069.
16 R. Nandi, H. K. Singh, S. K. Singh, B. Singh and R. K. Singh, *Spectrochim. Acta, Part A*, 2014, **128**, 248–256.
17 K. Vikram, S. K. Srivastava, A. K. Ojha, S. Schlücker, W. Kiefer and R. K. Singh, *J. Raman Spectrosc.*, 2009, **40**, 881–886.
18 K. Vikram, P. R. Alapati and R. K. Singh, *Spectrochim. Acta, Part A*, 2010, **75**, 1480–1485.
19 R. Ogawa, Y. Miwa and S. Kutsumizu, *J. Phys. Chem. B*, 2015, **119**, 10131–10137.
20 J. F. Bardeau, A. N. Parikh, J. D. Beers and B. I. Swanson, *J. Phys. Chem. B*, 2000, **104**, 627–635.
21 M. J. Frisch, G. W. Trucks, H. B. Schlegel, G. E. Scuseria, J. R. Cheeseman, M. A. Robb, G. Scalmani, V. Barone, B. Mennucci, G. A. Petersson, H. Nakatsuji, M. Caricato, X. Li, H. P. Hratchian, A. F. Izmzylov, J. Bloino, G. Zheng, J. L. Sonnenberg, M. Hada, M. Ehara, K. Toyota, R. Fukuda, J. Ishida, M. Hasegawa, T. Nakajima, Y. Honda, O. Kitao, H. Nakai, T. Vreven, J. A. Montgomery Jr., J. E. Peralta, F. Ogliaro, M. Bearpark, J. J. Heyd, E. Brothers, K. N. Kudin, V. N. Staroverov, R. Kobayashi, J. Normand, A. Raghavachari, A. Rendell, J. C. Burant, S. S. Iyengar, J. Tomasi, M. Cossi, N. Rega, J. M. Millan, M. Klene, J. E. Knox, J. B. Cross, V. Bakken, C. Adamo, J. Jaramillo, R. Gomperts, R. E. Stratmann, O. Yazyev, A. J. Austin, R. Cammi, C. Pomelli, J. W. Ochterski, R. L. Martin, K. Morokuma, V. G. Zakrzewski, G. A. Voth, P. Salvador, J. J. Dannerberg, S. Dapprich, A. D. Daniels, J. Farkas, B. Foresman, J. V. Ortiz, J. Cioslowski and D. J. Fox, *GAUSSIAN 09, Revision*, Gaussian, Inc., Wallingford, CT, 2009.
22 C. T. Lee, W. T. Yang and R. G. Parr, *Phys. Rev. B*, 1988, **37**, 785–789.
23 R. G. Parr and W. Yang, *Density Functional Theory of Atoms and Molecules*, Oxford University Press, New York, 1989.
24 A. D. Becke, *J. Chem. Phys.*, 1993, **98**, 5648–5652.
25 G. A. Petersson and M. A. Allaham, *J. Chem. Phys.*, 1991, **94**, 6081–6090.
26 G. A. Petersson, A. Bennett, T. G. Tensfeldt, M. A. Allaham, W. A. Shirley and J. Mantzaris, *J. Chem. Phys.*, 1988, **89**, 2193–2218.
27 P. Pulay, G. Fogarasi, F. Pang and J. E. Boggs, *J. Am. Chem. Soc.*, 1979, **101**, 2550–2560.
28 G. Fogarasi, X. Zhou, P. W. Taylor and P. Pulay, *J. Am. Chem. Soc.*, 1992, **114**, 8191–8201.
29 A. P. Scott and L. Radom, *J. Phys. Chem.*, 1996, **100**, 16502–16513.
30 J. M. L. Martin and C. V. Alsenoy, *Gar2ped*, University of Antwerp, 1995.
31 G. A. Zhurko and D. A. Zhurko, Chemcraft <http://www.chemcraftprog.com>, 2005.
32 A. Frisch, A. B. Nielson and A. J. Holder, *Gauss View User Manual*, Gaussian Inc., Pittsburgh, PA, 2000.
33 Y.-K. Kim, G. Cukrov, J. Xiang, S.-T. Shin and O. D. Lavrentovich, *Soft Matter*, 2015, **11**, 3963–3970.
34 N. Vaupotič, J. Szydlowska, M. Salamonczyk, A. Kovarova, J. Svoboda, M. Osipov, D. Pociecha and E. Gorecka, *Phys. Rev. E*, 2009, **80**, 030701(R).
35 N. V. S. Rao, R. Deb, M. K. Paul and T. Francis, *Liq. Cryst.*, 2009, **36**, 977–987.
36 N. Begum, S. Turlapati, S. Debnath, G. Mohiuddin, D. D. Sarkar and N. V. S. Rao, *Liq. Cryst.*, 2013, **40**, 1105–1115.
37 P. Tandon, G. Forster, R. Neubert and S. Wartewig, *J. Mol. Struct.*, 2000, **524**, 201–215.
38 N. V. S. Rao, M. K. Paul, I. Miyake, Y. Takanishi, K. Ishikawa and H. Takezoe, *J. Mater. Chem.*, 2003, **13**, 2880–2884.
39 R. G. Snyder, in *Methods of Experimental Physics*, ed. L. Marton and C. Marton, Academic Press, New York, 1980.
40 R. G. Snyder, *J. Mol. Spectrosc.*, 1960, **4**, 411–434.
41 L. Senak, D. Moore and R. Mendelsohn, *J. Phys. Chem.*, 1992, **96**, 2749–2754.
42 C. Naselli, J. P. Rabe, J. F. Rabolt and J. D. Swalen, *Thin Solid Films*, 1985, **134**, 173–178.
43 J. F. Bardeau, A. N. Parikh, J. D. Beers and B. I. Swanson, *J. Phys. Chem. B*, 2000, **104**, 627–635.
44 B. J. Bulkin and N. Krishnan, *J. Am. Chem. Soc.*, 1971, **93**, 5998.
45 S. K. Dash, R. K. Singh, P. R. Alapati and A. L. Verma, *J. Phys.: Condens. Matter*, 1997, **9**, 7809–7815.